HHS Public Access

Author manuscript

Oncogene. Author manuscript; available in PMC 2021 February 17.

Published in final edited form as:

Oncogene. 2020 September ; 39(38): 6129–6137. doi:10.1038/s41388-020-01424-7.

Cancer-associated fibroblasts downregulate type I interferon receptor to stimulate intra-tumoral stromagenesis

Christina Cho[1], **Riddhita Mukherjee**[1], **Amy R. Peck**[2], **Yunguang Sun**[2], **Noreen McBrearty**[1], **Kanstantsin V. Katlinski**[1], **Jun Gui**[1], **Priya K. Govindaraju**[1], **Ellen Puré**[1], **Hallgeir Rui**[2], **Serge Y. Fuchs**[1,@]

[1]Department of Biomedical Sciences, School of Veterinary Medicine, University of Pennsylvania, Philadelphia, PA 19104, USA

[2]Department of Pathology, Medical College of Wisconsin, Milwaukee, WI 53226, USA

Abstract

Activation of cancer-associated fibroblasts (CAFs) and ensuing desmoplasia play an important role in the growth and progression of solid tumors. Here we demonstrate that, within colon and pancreatic ductal adenocarcinoma tumors, efficient stromagenesis relies on downregulation of the IFNAR1 chain of type I interferon (IFN1) receptor. Expression of the fibroblast activation protein (FAP) and accumulation of the extracellular matrix (ECM) was notably impaired in tumors grown in the *Ifnar1*^{S526A} (SA) knock-in mice, which are deficient in IFNAR1 downregulation. Primary fibroblasts from these mice exhibited elevated levels of Smad7, a negative regulator of the tumor growth factor-beta (TGFβ) pathway. Knockdown of Smad7 alleviated deficient ECM production in SA fibroblasts in response to TGFβ. Analysis of human colorectal cancers revealed an inverse correlation between IFNAR1 and FAP levels. Whereas growth of tumors in SA mice was stimulated by co-injection of wild type but not SA fibroblasts, genetic ablation of IFNAR1 in fibroblasts also accelerated tumor growth. We discuss how inactivation of IFNAR1 in CAFs acts to stimulate stromagenesis and tumor growth.

Keywords

Cancer associated fibroblast; desmoplasia; interferon; IFNAR1; stromagenic switch; fibroblast activation protein; transforming growth factor-beta; tumor growth

INTRODUCTION

Solid tumors grow in a complex and dynamic microenvironment populated by various types of cells [1]. Cancer-associated fibroblasts (CAFs) make up a large proportion of the cell population within the tumor microenvironment [2], and the presence of CAFs in the stroma

@Correspondence to Serge Y. Fuchs, syfuchs@upenn.edu.

CONFLICT OF INTEREST

None to report.

has been associated with poor prognosis in many cancers, such as colorectal and pancreatic ductal adenocarcinomas (reviewed in [3, 4]). Protumorigenic activities of CAFs are mediated by a number of mechanisms, including secretion of growth factors and cytokines that promote malignant cell proliferation and immune evasion [5–8]. Furthermore, CAFs deposit and remodel the extracellular matrix (ECM) to generate a growth-supportive desmoplastic stroma [4, 9, 10]. Emerging evidence that support the pro-tumorigenic functions of CAFs have warranted the development and use of CAF-targeted therapies for cancer treatment [11–14] and prompted additional studies towards a better understanding of the molecular mechanisms driving the generation and activities of CAFs.

The stromagenic switch is the process in which resident and recruited fibroblasts are pathologically activated into CAFs [15]. A well-established inducer of CAFs activation is TGFβ [16, 17], whose signaling activity culminates in the upregulation of several CAF surface markers, including fibroblast activation protein (FAP) [18]. Although the TGFβ pathway is tightly regulated under physiological conditions, such as wound healing, it is dysregulated in the tumor microenvironment. While activated fibroblasts revert back to normal fibroblasts upon completion of wound healing, CAFs remain reprogrammed and pathologically activated throughout tumor progression [4, 9]. Therefore, it is likely, that under normal conditions, there exists a mechanism which acts to prevent the constitutive activation of fibroblasts. Moreover, this prohibitive mechanism is likely inactivated during tumor growth. Here we present data indicating that inactivation of the IFNAR1 chain of the Type I interferons (IFN1) receptor contributes to activation of CAFs and ensuing desmoplasia.

IFN1 are anti-tumor cytokines that signal and then elicit a massive reprogramming of transcriptional activities; all effects of IFN1 are mediated through the heterodimeric receptor complex composed of IFNAR1 and IFNAR2 chains [19, 20]. Tumors evade the IFN1 pathway by downregulating IFNAR1 in all types of cells within the tumor microenvironment, including intra-tumoral fibroblasts [21, 22]. Mice that express mutant IFNAR1 protein, which is deficient in its ubiquitination and, therefore, remain stable (*Ifnar1*^{S526A}, [23], henceforth termed "**SA**") poorly support growth of solid tumors [22, 24]. Previously, we demonstrated that downregulation of IFNAR1 in the intra-tumoral cytotoxic T lymphocytes induces the formation of an immune-privileged niche in human colorectal cancers (CRC) and a mouse model of colon adenocarcinoma [22]. In the present study, we investigated the importance of IFNAR1 inactivation in the non-immune tumor stroma.

RESULTS

Within solid tumors, tumor microenvironment stress (e.g. inflammatory stimuli and hypoxia) downregulated IFNAR1 and inactivated the IFN1 pathway within all types of cells [22]. Downregulation of IFNAR1 in the host promoted growth of subcutaneous tumors formed by colon (MC38, Figure 1A) and pancreatic (MH6499c4, Figure 1B) adenocarcinoma cells as evident from delayed tumor growth in SA mice. Although inactivation of IFNAR1 in cytotoxic (CD8+) T cells plays an important role in this phenotype [22], we noticed that SA mice deficient in *Rag1* and, accordingly, lacking lymphocytes, also exhibited decelerated tumor growth (Figure 1C). Furthermore, SA mice reconstituted with wild type (WT) bone

marrow (WT>SA; Figure 1D) displayed limited tumor growth compared to WT chimeric recipients (WT>WT; Figure 1E). Collectively, these results suggest that downregulation of IFNAR1 in non-immune stromal cells is also important for robust tumor growth.

Examination of the stromal compartment in colon (Figure 2A) or pancreatic (Figure 2B) adenocarcinoma tumors revealed that tumors growing in SA hosts harbor developed limited stromagenesis. This phenotype was manifested by decreased levels of ECM components including fibronectin, versican and hyaluronic acid. Furthermore, the levels of FAP, an important marker of reactive/inflammatory CAFs [7] were lower in tumors growing in either SA mice (Figures 2A–B) or in chimeric SA mice transplanted with WT bone marrow (Figure 2C) indicating that intratumoral loss of IFNAR1 in the stroma promotes accumulation of CAFs. Together, these results suggest a role for IFNAR1 downregulation in the stromagenic switch and generation of pro-tumorigenic environment.

To test whether inactivation of IFN1 signaling is required for the stromagenic switch, we generated fibroblast-derived matrices (FDM) [25] using WT fibroblasts, in which IFNAR1 is readily degraded, or SA fibroblasts, in which IFNAR1 expression is preserved. While WT-FDM were abundant in fibronectin, SA-FDM were significantly less desmoplastic (Figure 2D). IFNγ was shown to induce a negative regulator of the TGFβ pathway, Smad7, in a manner that requires STAT1 [26], which is also activated by IFN1. Accordingly, attenuated production of fibronectin by SA fibroblasts coincided with increased levels of Smad7 (Figure 2D). Moreover, stimulation of IFN1 signaling in WT fibroblasts was sufficient to induce Smad7 expression (Figure 2E), while knockdown of Smad7 in SA fibroblasts restored their ability to generate a fibronectin-dense desmoplastic matrix (Figure 2F). These data suggest that inactivation of IFNAR1 in fibroblasts stimulates the stromagenic switch – at least in part through limiting Smad7 expression.

Importantly, in human CRC tumor tissues, the intra-tumoral stromal areas lacking IFNAR1 exhibited notably high expression of FAP (Figure 3A–C). Analysis of cells within the entire stromal compartment of human CRC showed almost mutually exclusive expression of FAP and IFNAR1 (Figure 3D–F). These results further suggest the importance of inactivation of IFNAR1 for the stromagenic switch and, given that low IFNAR1 [22] and high levels of FAP [27, 28] are associated with poor prognosis, argue for the importance of inactivation of IFNAR1 specifically in fibroblasts for supporting robust tumor growth.

To test the role of downregulation of IFNAR1 in the pro-tumorigenic capacity of CAFs, we utilized two complementary approaches. First, we co-injected primary WT or SA fibroblasts along with MC38 tumor cells into SA mice. Supplementation of MC38 cells with WT (but not SA) fibroblasts accelerated tumor growth (Figure 3G). This result indicates that IFNAR1 downregulation within fibroblasts plays a role in establishing a pro-tumorigenic environment.

These results were corroborated by experiments involving a second independent approach, where we ablated IFNAR1 specifically in fibroblasts by tamoxifen treatment of *Col1a2-CreER, Ifnar1*$^{fl/fl}$ animals to generate *Ifnar1*$^{\Delta fib}$ mice (Figure 3H–I). Analysis of tumor growth in these animals revealed that ablation of IFNAR1 notably increased the size of

tumors (Figure 3J). In these studies, tumors from *Ifnar1*$^{\Delta fib}$ mice exhibited a modest yet significant increase in FAP expression compared to tumors of comparable size grown for a longer time in *Ifnar1*$^{fl/fl}$ mice (Figure 3K). This increase is probably underestimated given that proteolytic downregulation of IFNAR1 in WT CAFs should blur the distinction with genetic ablation of IFNAR1. Altogether, these results suggest that inactivation of IFNAR1 in CAFs is required for their ability to support efficient tumor growth.

DISCUSSION

Our data indicate that proteolytic loss of IFNAR1 in the non-immune tumor microenvironment promoted stromagenesis and enhanced tumor growth, whereas stabilization of the receptor attenuated the pro-tumorigenic phenotype of CAFs. In human CRC tumors, IFNAR1 expression was spatially segregated from regions of high FAP expression, further demonstrating that loss of IFNAR1 is required for the pathological activation of CAFs. Altogether, these results suggest a novel mechanism by which the inactivation of the IFN1-IFNAR1 pathway enables the stromagenic switch and stimulates CAF-mediated tumor growth.

Inactivation of IFNAR1 and ensuing suppression of the IFN1 pathway in intra-tumoral cytotoxic T lymphocytes was shown to undermine their viability and drive the generation of an immune privileged niche within the tumor microenvironment [22]. In the present study, data obtained in experimental models that utilize bone marrow chimeras or animals lacking lymphocytes argue for the importance of IFNAR1 downregulation in the stromal compartment for tumor growth. The non-immune stromal compartment includes endothelial cells and fibroblasts. We noticed that angiogenesis was moderately inhibited in tumors grown in SA hosts (data not shown), and these results are consistent with importance of CAFs for activation of the endothelial cells [29] as well as with requirement of IFNAR1 downregulation for efficient VEGF-driven angiogenesis [30]. Thus, we cannot rule out additional importance of IFNAR1 inactivation in the endothelial cells in stimulation of tumor growth. However, based on experiments that involved IFNAR1 modulation specifically in fibroblasts, this study clearly points to the importance of downregulation of IFNAR1 in the activation and stromagenic function of CAFs. Future studies are warranted to examine the association between IFNAR1 levels in CAFs with immune infiltration of human tumors and potential responses to immunotherapies.

Results from our pre-clinical models of colon and pancreatic ductal adenocarcinoma tumors paralleled the data obtained in samples from human patients. Both showed that IFNAR1 expression in the tumor stroma was associated with low FAP expression. Considering that high FAP [27, 28] and low IFNAR1 [22] expression are associated with poor prognosis, our studies demonstrate the importance of IFNAR1 loss in intratumoral FAP^{+} inflammatory fibroblasts for their ability to support tumor progression.

Whereas our data implicate IFN1-induced expression of Smad7 as a potential mechanism mediating IFN1-driven suppression of stromagenesis, other putative mechanisms that could be inactivated within the tumor microenvironment cannot be ruled out. For example, downregulation of IFNAR1 promotes the uptake of the tumor-derived extracellular vesicles

[31], which have been shown to stimulate activation of CAFs and ensued stromagenesis [32, 33].

The expression of the IL-1 receptor (IL1R1) is required for the pro-tumorigenic CAF phenotype [16], and IL-1 promotes downregulation of IFNAR1 in a manner that depends on activity of p38α protein kinase [34]. Intriguingly, recent studies of stromagenesis within pulmonary pre-metastatic niche suggested that p38-driven downregulation of IFNAR1 is essential for expression of FAP in the lungs of mice treated with the tumor-derived factors. Furthermore, these studies showed that decelerated tumor growth in mice lacking p38α in fibroblasts could be reverted by ablation of IFNAR1 [35].

Future studies will determine whether the blockade of the IL-1/IL1R1 and/or p38α pathways may stabilize IFNAR1 expression in fibroblasts and ultimately inhibit the stromagenic switch and CAFs-stimulated tumor growth. As desmoplasia promotes chemo-resistance in solid tumors; targeting the stromagenesis may improve the efficacy of anti-tumor therapies [36]. Accordingly, therapeutic modalities that stabilize IFNAR1 and re-activate the IFN1 pathway in fibroblasts may help to achieve this goal.

MATERIALS AND METHODS

Mouse Studies

All mouse experiments were approved by the Institutional Animal Care and Use Committee (IACUC) of The University of Pennsylvania. Mice were maintained in a specific pathogen-free facility in accordance with the American Association for Laboratory Animal Science guidelines. All mice were of C57BL/6NJ background, and unless otherwise described are 6-8 weeks of age. Mice of both sexes were utilized for these studies. *Rag1*$^{-/-}$, *Ifnar1*$^{fl/fl}$, and *Col1a2-Cre*$^{ERT2/+}$ mice were obtained from Jackson Laboratory (Bar Harbor, ME, USA). *Ifnar1*^{S526A} mice ("SA") and bone marrow chimeras were generated as previously described [23]. Fibroblast-specific IFNAR1 knockout mice (*Ifnar1*$^{\Delta fib}$) were established by crossing *Ifnar1*$^{fl/fl}$ mice with *Col1a2-Cre*$^{ERT2/+}$ mice. The resultant *Col1a2-Cre*$^{ERT2/+}$; *Ifnar1*$^{fl/fl}$ mice were genotyped by PCR (Figure 3I). The *Col1a2-Cre*$^{ERT2/+}$ was induced by administering tamoxifen (Sigma #T5648, St. Louis, MO, USA) 0.2 mg/g, daily for 5 days. Deletion of IFNAR1 was confirmed by PCR with primers for mouse wildtype IFNAR1 (Forward: 5'-CTGGGAGCCAGGGCATAAC-3', Reverse 5'-CCAGCCTTTCGGAGTGTGC-3') (Figure 3I). Littermates were randomly assigned into experimental groups, which were either co-housed or exposed to other groups' bedding to ensure exposure to all groups' microbiota.

Cell culture

MC38, NIH3T3 and HEK293T cells were maintained at 37°C with 5% CO2 in DMEM supplemented with 10% FBS, penicillin, and streptomycin. MH6499c4 mouse PDA cells were gifted by Dr. Ben Stanger from the University of Pennsylvania (Philadelphia) and maintained as previously described [37]. All cell lines were tested for mycoplasma contamination and were confirmed to be mycoplasma-free. For isolation of primary mouse fibroblasts, lungs harvested from 3- to 5-week-old mice were dissociated in PBS containing 100mg Collagenase II (Worthington #LS004202, Lakewood, NJ, USA) and 5mg DNAse I

(Sigma #10104159001) and passed through 100 and 40 μm cell strainers to obtain single-cell suspensions. Fibroblasts were cultured for 20 minutes at 37°C, then non-adherent cells were washed off.

Immunohistochemical and immunofluorescent analysis of tumor tissues

OCT-embedded, frozen tumor tissues were cryosectioned in a Leica CM3050 S Cryostat at 10μm thickness for all immunohistochemical (IHC) and immunofluorescence (IF) studies. Slides were incubated overnight in primary antibody at 4°C. Secondary/tertiary antibodies were added and sections were developed and counterstained according to the appropriate protocol. For IHC, the following antibodies were used: anti-human fibronectin (Sigma #F3648), anti-mouse versican (EMD Millipore #AB1033, Burlington, MA, USA), biotinylated hyaluronic acid binding protein, HABP (EMD Millipore #385911), Rabbit IgG isotype control (Santa Cruz Biotechnology #sc-2027, Dallas, TX, USA), and biotin-SP-conjugated goat anti-rabbit IgG secondary antibody (Jackson Immunoresearch #AB2337959, West Grove, PA, USA). The following antibodies were used for IF: anti-human FAP antibody (R&D Systems #AF3715, Minneapolis, MN, USA or Abcam #53066, Cambridge, MA, USA) or sheep IgG isotype control (R&D Systems #5001A), and AF488-conjugated donkey anti-sheep IgG secondary antibody (ThermoFisher #A11015, Waltham, MA, USA). All imaging was completed with the Olympus Spot-RT3 microscope at 20X magnification. For quantification purposes, 3-5 different tumor samples ($n \geq 3$) from each experimental group were used. The mean area of positive staining and mean fluorescence intensity were determined using Fiji ImageJ Software.

Western Blot Analysis

Cells treated with IFNβ (PBL Assay Science #12400-1, Piscataway, NJ, USA) and recombinant mouse TGFβ1 (R&D systems #7666-MB) were lysed in RIPA buffer and whole cell lysates were evaluated for SMAD7 expression by Western blot analysis as described [23] using indicated antibodies (Smad7, ThermoFisher #42-0400 and GAPDH, Cell Signaling Technologies #14C10, Danvers, MA , USA). Densitometric analysis of the protein bands was completed with Fiji Image J.

FDM generation and analysis

Non-extracted (containing cells) FDMs were generated (as described in [25]) and analyzed for their expression of Fibronectin and Smad7 by immunofluorescence using antibodies against fibronectin (Sigma #F3648), Smad7 (ThermoFisher #42-0400), AF488-conjugated goat-anti-rabbit IgG (ThermoFisher #A11070) or AF594 conjugated anti-rabbit IgG (ThermoFisher #A11072). Imaging was completed with the Olympus Spot-RT3 microscope at 20X magnification. For quantification, 4-5 different fields of view of each type of matrix were used, and the matrix assembly assay was completed at least 3 independent times. The total area of positive FN staining and the % of SMAD7-positive nuclei was determined using ImageJ software. To calculate the % of SMAD7-positive nuclei, the following formula was utilized: (# of SMAD7 particles ÷ # of DAPI-stained nuclei) x 100%.

Lentiviral-mediated knockdown of SMAD7 in SA lung fibroblasts

pLKO-.1-shSMAD7 and pLKO.1-control plasmids [38] were gifted by Dr. Xin-Hua Feng (Zheijiang University, Hangzhou, China). For lentiviral production, 293T cells were transfected with pLKO-.1-shSMAD7 or pLKO.1-control plasmids followed by lentivirus harvest and transduction of SA fibroblasts as previously described [34].

Analysis of human cancers and statistical analysis

A human CRC tissue microarray (Cat# CRM1505) containing 150 cases of formalin-fixed, paraffin-embedded CRC cancer was obtained from US Biomax, Inc (Rockville, MD, USA). IF/IHC was performed as previously described [39] to detect IFNAR1 and FAP on a single slide using the following conditions: antigen retrieval with Tris/EDTA buffer pH 9.0, and incubation with rabbit polyclonal IFNAR1 antibody (Sigma, HPA018015), rabbit monoclonal FAP antibody (Abcam #ab207178), and mouse monoclonal anti-pan-cytokeratin (Agilent #M351501-2). Quantitative analysis was performed as previously described [39] using the Panoramic 250 Flash II slide scanner (3DHISTECH Ltd., Budapest, Hungary) to capture high-resolution digital images followed by quantification of biomarker levels using Tissue Studio image analysis software (Definiens, Munich, Germany). Mean biomarker signal intensity per cell was calculated for epithelial and stromal regions. Scatterplot of IFNAR1 and FAP signal intensities within each cell were generated per patient core. Representative cases shown.

Quantification and Statistical Analysis

All data are presented as mean ± s.e.m or mean ± s.d. (as indicated) of at least three biological replicates. Statistical analysis was performed using GraphPad Prism 8 software (GraphPad Prism Software Inc). Unpaired t-tests, or paired ratio t-tests were used for comparisons between two groups. One-way ANOVA or two-way ANOVA analyses followed by the Tukey post-hoc tests were used for multiple comparisons.

ACKNOWLEDGEMENTS

This work was supported by the by the NIH/NCI R01 grants CA092900 (to S.Y.F.), CA240814 (to S.Y.F. and H.R.) and P01 CA217805 (to E.P.). Additional support from T32 CA115299 (to N.M.) and T32 CA009140 (to K.V.K.) is also greatly appreciated.

We would like to thank Dr. Ben Z. Stanger and Jinyang Li for generously gifting mouse PDA cells and advising us in the generation of PDAC subcutaneous tumors. We also thank Drs. Xin Hua Feng and Yi Yu and for generously gifting the pLKO.1 plasmids, and providing the protocols for generating the aforementioned lentiviruses.

REFERENCES

1. Hanahan D, Coussens LM. Accessories to the Crime: Functions of Cells Recruited to the Tumor Microenvironment. Cancer Cell, vol. 21, 2012, pp 309–322. [PubMed: 22439926]
2. Sahai E, Astsaturov I, Cukierman E, DeNardo DG, Egeblad M, Evans RM et al. A framework for advancing our understanding of cancer-associated fibroblasts. Nature Reviews Cancer 2020; 20: 174–186. [PubMed: 31980749]
3. Gascard P, Tlsty TD. Carcinoma-associated fibroblasts: orchestrating the composition of malignancy. Genes Dev 2016; 30: 1002–1019. [PubMed: 27151975]

4. Alexander J, Cukierman E. Stromal dynamic reciprocity in cancer: Intricacies of fibroblastic-ECM interactions Current Opinion in Cell Biology, vol. 42 Elsevier Ltd, 2016, pp 80–93. [PubMed: 27214794]
5. Erdogan B, Webb DJ. Cancer-associated fibroblasts modulate growth factor signaling and extracellular matrix remodeling to regulate tumor metastasis. Biochemical Society Transactions 2017; 45: 229–236. [PubMed: 28202677]
6. Kato T, Noma K, Ohara T, Kashima H, Katsura Y, Sato H et al. Cancer-associated fibroblasts affect intratumoral CD8+ and Foxp3+ T cells via IL6 in the tumor microenvironment. Clinical Cancer Research 2018; 24: 4820–4833. [PubMed: 29921731]
7. Öhlund D, Handly-Santana A, Biffi G, Elyada E, Almeida AS, Ponz-Sarvise M et al. Distinct populations of inflammatory fibroblasts and myofibroblasts in pancreatic cancer. The Journal of Experimental Medicine 2017; 214: 579–596. [PubMed: 28232471]
8. Zhang R, Qi F, Zhao F, Li G, Shao S, Zhang X et al. Cancer-associated fibroblasts enhance tumor-associated macrophages enrichment and suppress NK cells function in colorectal cancer. Cell Death and Disease 2019; 10.
9. DA Beacham EC. Stromagenesis: the changing face of fibroblastic microenvironments during tumor progression. Semin Cancer Biol 2005; 15: 329–341. [PubMed: 15970443]
10. Goetz JG, Minguet S, Navarro-Lérida I, Lazcano JJ, Samaniego R, Calvo E et al. Biomechanical remodeling of the microenvironment by stromal caveolin-1 favors tumor invasion and metastasis. Cell 2011; 146: 148–163. [PubMed: 21729786]
11. Feig C, Jones JO, Kraman M, Wells RJB, Deonarine A, Chan DS et al. Targeting CXCL12 from FAP-expressing carcinoma-associated fibroblasts synergizes with anti-PD-L1 immunotherapy in pancreatic cancer. Proceedings of the National Academy of Sciences of the United States of America 2013; 110: 20212–20217. [PubMed: 24277834]
12. Lo A, Wang LS, Scholler J, Monslow J, Avery D, Newick K et al. Tumor-Promoting Desmoplasia Is Disrupted by Depleting FAP-Expressing Stromal Cells. Cancer Res 2015; 75: 2800–2810. [PubMed: 25979873]
13. Santos AM, Jung J, Aziz N, Kissil JL, Puré E. Targeting fibroblast activation protein inhibits tumor stromagenesis and growth in mice. Journal of Clinical Investigation 2009; 119: 3613–3625. [PubMed: 19920354]
14. Wang LCS, Lo A, Scholler J, Sun J, Majumdar RS, Kapoor V et al. Targeting fibroblast activation protein in tumor stroma with chimeric antigen receptor T cells can inhibit tumor growth and augment host immunity without severe toxicity. Cancer Immunology Research 2014; 2: 154–166. [PubMed: 24778279]
15. Puré E, Lo A. Can targeting stroma pave the way to enhanced antitumor immunity and immunotherapy of solid tumors? Cancer Immunology Research 2016; 4: 269–278. [PubMed: 27036971]
16. Biffi G, Oni TE, Spielman B, Hao Y, Elyada E, Park Y et al. Il1-induced Jak/STAT signaling is antagonized by TGFβ to shape CAF heterogeneity in pancreatic ductal adenocarcinoma. Cancer Discovery 2019; 9: 282–301. [PubMed: 30366930]
17. Calon A, Tauriello DVF, Batlle E. TGF-beta in CAF-mediated tumor growth and metastasis Seminars in Cancer Biology, vol. 25 Academic Press, 2014, pp 15–22. [PubMed: 24412104]
18. Chen H, Yang WW, Wen QT, Xu L, Chen M. TGF-β-induced fibroblast activation protein expression, fibroblast activation protein expression increases the proliferation, adhesion, and migration of HO-8910PM. Experimental and Molecular Pathology 2009; 87: 189–194. [PubMed: 19747910]
19. Fish EN, Platanias LC. Interferon receptor signaling in malignancy: A network of cellular pathways defining biological outcomes. Molecular Cancer Research 2014; 12: 1691–1703. [PubMed: 25217450]
20. Piehler J, Thomas C, Christopher Garcia K, Schreiber G. Structural and dynamic determinants of type I interferon receptor assembly and their functional interpretation. Immunological Reviews 2012; 250: 317–334. [PubMed: 23046138]
21. Fuchs SY. Hope and fear for interferon: the receptor-centric outlook on the future of interferon therapy. J Interferon Cytokine Res 2013; 33: 211–225. [PubMed: 23570388]

22. Katlinski KV, Gui J, Katlinskaya YV, Ortiz A, Chakraborty R, Bhattacharya S et al. Inactivation of Interferon Receptor Promotes the Establishment of Immune Privileged Tumor Microenvironment. Cancer Cell 2017; 31: 194–207. [PubMed: 28196594]
23. Bhattacharya S, Katlinski KV, Reichert M, Takano S, Brice A, Zhao B et al. Triggering ubiquitination of IFNAR1 protects tissues from inflammatory injury. EMBO Molecular Medicine 2014; 6: 384–397. [PubMed: 24480543]
24. Katlinskaya YV, Katlinski KV, Yu Q, Ortiz A, Beiting DP, Brice A et al. Suppression of Type I Interferon Signaling Overcomes Oncogene-Induced Senescence and Mediates Melanoma Development and Progression. Cell Rep 2016; 15: 171–180. [PubMed: 27052162]
25. Castelló-Cros R, Cukierman E. Stromagenesis during tumorigenesis: characterization of tumor-associated fibroblasts and stroma-derived 3D matrices. Methods in Molecular Biology (Clifton, NJ) 2009; 522: 275–305.
26. Ulloa L, Doody J, Massague J. Inhibition of transforming growth factor-beta/SMAD signalling by the interferon-gamma/STAT pathway. Nature 1999; 397: 710–713. [PubMed: 10067896]
27. Henry LR, Lee HO, Lee JS, Klein-Szanto A, Watts P, Ross EA et al. Clinical implications of fibroblast activation protein in patients with colon cancer. Clinical Cancer Research 2007; 13: 1736–1741. [PubMed: 17363526]
28. Wikberg ML, Edin S, Lundberg IV, Van Guelpen B, Dahlin AM, Rutegård J et al. High intratumoral expression of fibroblast activation protein (FAP) in colon cancer is associated with poorer patient prognosis. Tumor Biology 2013; 34: 1013–1020. [PubMed: 23328994]
29. Lieberman A, Barrett R, Kim J, Zhang KL, Avery D, Monslow J et al. Deletion of Calcineurin Promotes a Protumorigenic Fibroblast Phenotype. Cancer Res 2019; 79: 3928–3939. [PubMed: 31189649]
30. Zheng H, Qian J, Carbone CJ, Leu NA, Baker DP, Fuchs SY. Vascular endothelial growth factor-induced elimination of the type 1 interferon receptor is required for efficient angiogenesis. Blood 2011; 118: 4003–4006. [PubMed: 21832278]
31. Ortiz A, Gui J, Zahedi F, Yu P, Cho C, Bhattacharya S et al. An Interferon-Driven Oxysterol-Based Defense against Tumor-Derived Extracellular Vesicles. Cancer Cell 2019; 35: 33–45. [PubMed: 30645975]
32. Webber J, Steadman R, Mason MD, Tabi Z, Clayton A. Cancer exosomes trigger fibroblast to myofibroblast differentiation. Cancer Research 2010; 70: 9621–9630. [PubMed: 21098712]
33. Webber JP, Spary LK, Sanders AJ, Chowdhury R, Jiang WG, Steadman R et al. Differentiation of tumour-promoting stromal myofibroblasts by cancer exosomes. Oncogene 2015; 34: 319–333.
34. Huangfu WC, Qian J, Liu C, Liu J, Lokshin AE, Baker DP et al. Inflammatory signaling compromises cell responses to interferon alpha. Oncogene 2012; 31: 161–172. [PubMed: 21666722]
35. Gui J, Zahedi F, Ortiz A, Cho C, Katlinski KV, Alicea-Torres K et al. Activation of p38α stress-activated protein kinase drives the formation of the pre-metastatic niche in the lungs. Nat Cancer 2020; Nat Cancer, 1: 603–619.
36. Valkenburg KC, de Groot AE, Pienta KJ. Targeting the tumour stroma to improve cancer therapy. Nat Rev Clin Oncol 2018; 15: 366–381. [PubMed: 29651130]
37. Li J, Byrne KT, Yan F, Yamazoe T, Chen Z, Baslan T et al. Tumor Cell-Intrinsic Factors Underlie Heterogeneity of Immune Cell Infiltration and Response to Immunotherapy. Immunity 2018; 49: 178–193.e177. [PubMed: 29958801]
38. Yu Y, Gu S, Li W, Sun C, Chen F, Xiao M et al. Smad7 enables STAT3 activation and promotes pluripotency independent of TGF-β signaling. Proceedings of the National Academy of Sciences of the United States of America 2017; 114: 10113–10118. [PubMed: 28874583]
39. Peck AR, Girondo MA, Liu C, Kovatich AJ, Hooke JA, Shriver CD et al. Validation of tumor protein marker quantification by two independent automated immunofluorescence image analysis platforms. Modern Pathology 2016; 29: 1143–1154. [PubMed: 27312066]

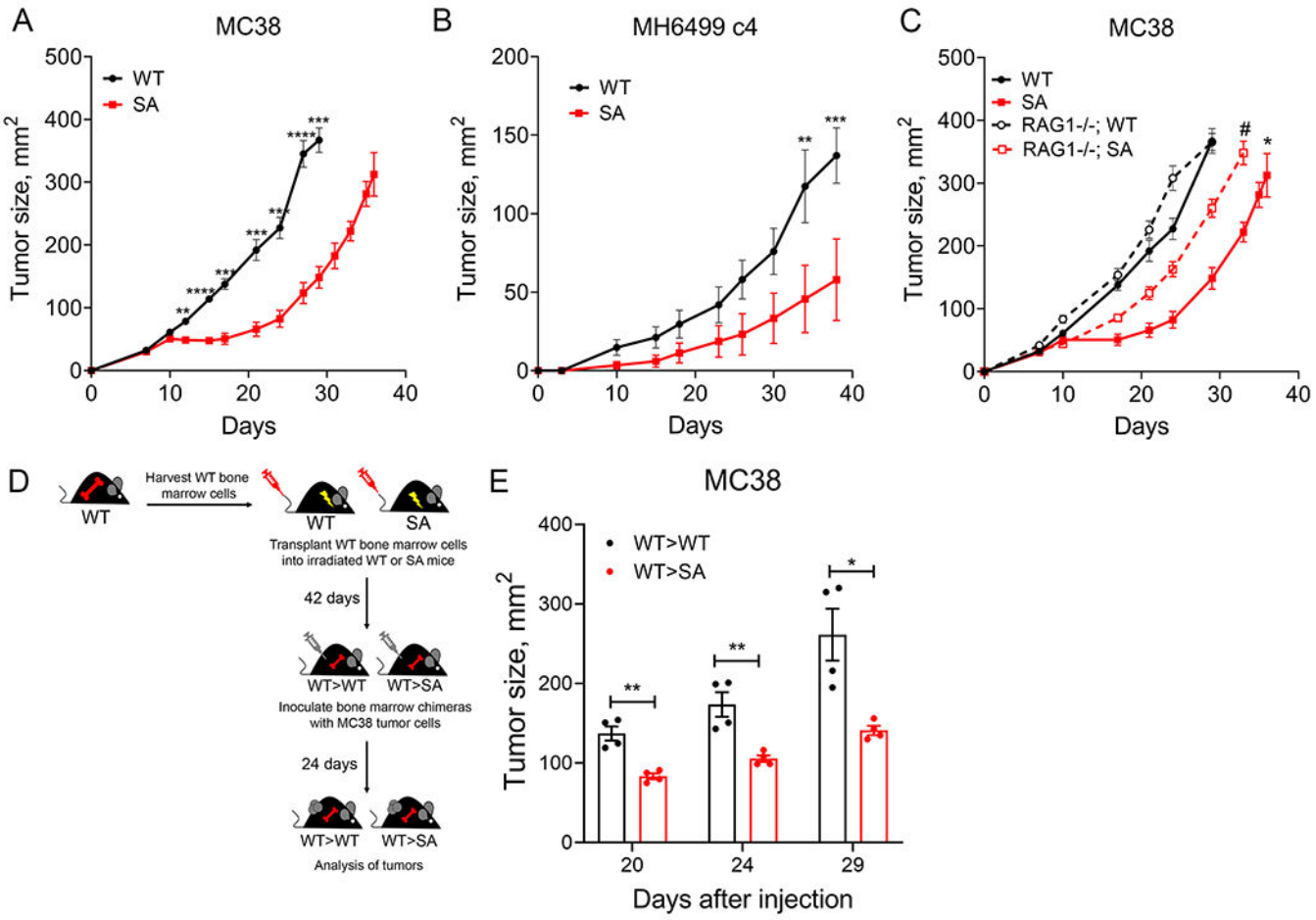

Figure 1. Inactivation of IFNAR1 in the non-immune tumor stroma promotes tumor growth.

(A) ***Growth of MC38 tumors is increased in WT mice compared to SA mice***. 10^6 MC38 cells were subcutaneously injected into the right flank of WT or SA mice (n=5 for each group). Tumors were measured by caliper and tumor area was calculated by multiplying the length and width. Each point in each line graph represents the mean ± S.D. tumor area (mm^2). Statistical significance was determined by two-way ANOVA (**p<0.05, ***p<0.005, ****p<0.0001).

(B) ***Growth of MH6499c4 tumors is increased in WT mice compared to SA mice.*** 10^5 MH6499c4 cells were subcutaneously injected into the right flank of WT (n=4) or SA (n=5) mice. Each point in each line graph represents the mean ± S.D. tumor area (mm^2). Statistical significance was determined by two-way ANOVA (**p<0.05, ***p<0.005).

(C) ***SA mice exhibit reduced tumor growth in the absence of lymphocytes.*** 10^6 MC38 cells were subcutaneously injected into the right flank of the indicated mice. Each point in each line graph represents the mean ± S.D. tumor area (mm^2); n=5 for each experimental group. Tumors grown in WT mice were significantly larger than SA mice (*p<0.05, n=5), and tumors in *$Rag1^{-/-}$; SA* were smaller than in *$Rag1^{-/-}$; WT* mice (#p<0.05, n=5). Statistical significance was determined by two-way ANOVA.

(D) ***A schematic describing the development of bone marrow chimeras***. Bone marrow cells were harvested from WT mice (donor). WT bone marrow cells were transplanted into

irradiated WT (WT>WT) or SA mice (WT>SA) via tail-vein injection. 42 days post-transplantation, chimeras were inoculated s.c. with 10^6 MC38 cells.

(E) ***Tumor growth is attenuated in WT>SA mice compared to WT>WT mice***. Each point within each bar graph represents the tumor size (mm^2) of a single mouse in each experimental group. Each bar represents the mean ± S.D in tumor size of four mice (n=4). Statistical significance was determined by student T-test (**p<0.05; ***p<0.005).

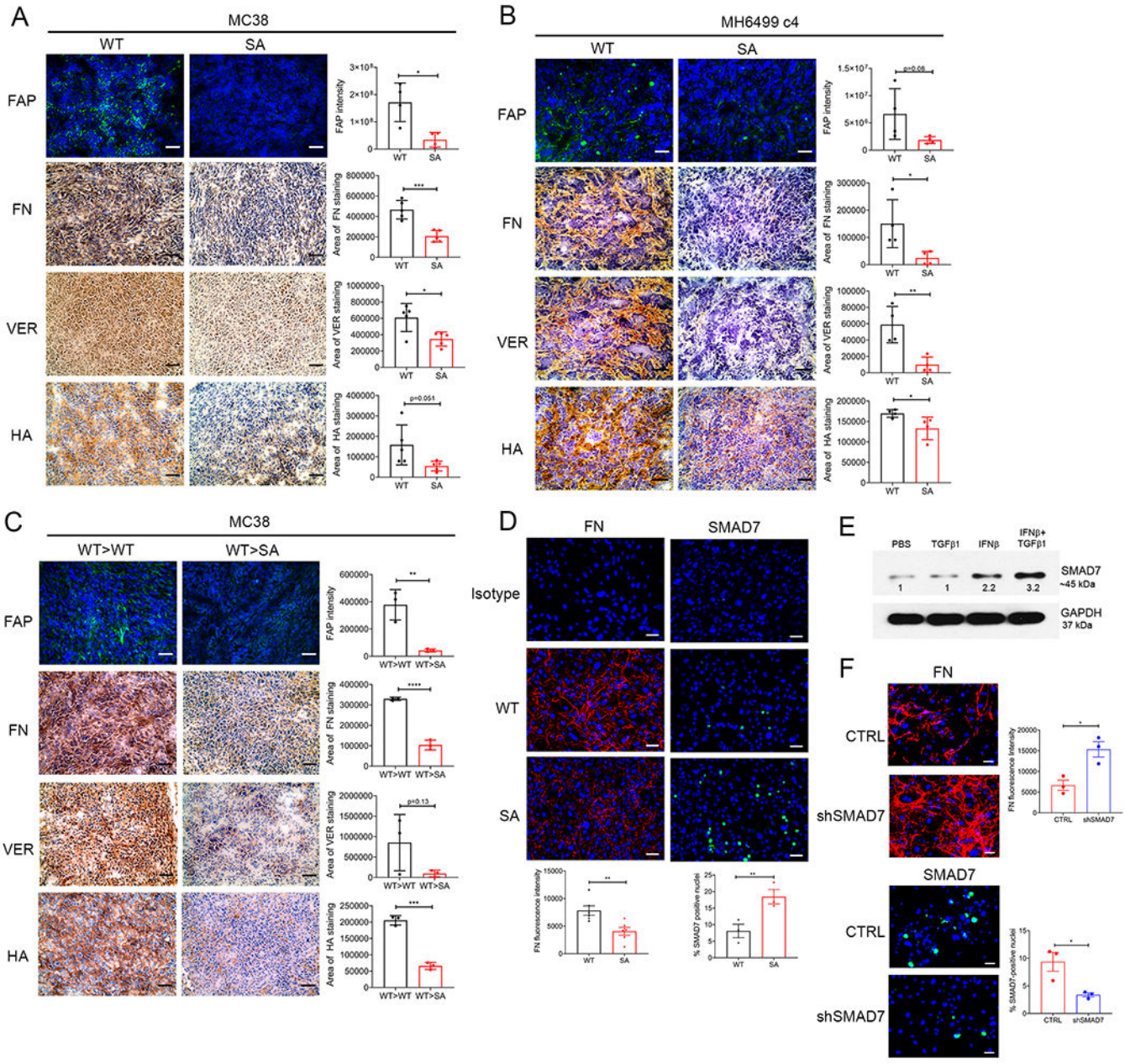

Figure 2. Downregulation of IFNAR1 in fibroblasts induces the stromagenic switch.

(A-B) ***Colon and pancreatic ductal adenocarcinoma tumors generated in SA mice exhibit reduced stromagenesis and FAP expression.*** The expression levels of the ECM proteins Fibronectin (FN), Versican (VER), and Hyaluronic Acid (HA) in tumors was analyzed by IHC. Expression of the inflammatory CAFs marker FAP was evaluated by IF. The area of positive staining is presented as mean ± S.D. of at least 4 individual tumors (n=5 for MC38 CRC and n=4 for MH6499c4 PDA) with each dot representing a biological replicate. Fluorescence intensity is presented as mean ± S.D of 4 individual tumors (n=4), with each dot representing a biological replicate. Statistical significance was determined by Unpaired

student t-tests (*p<0.05, **p<0.005, ***p<0.0005). All images were taken at 20X magnification. Scale bar = 50μm.

(C) ***Tumors derived from WT>SA mice exhibit lower levels of stromagenesis and FAP expression than tumors from WT>WT animals.*** The area of positive staining is presented as mean ± S.D. of 3 individual tumors (n=3) with each dot representing a biological replicate. Fluorescence intensity is presented as mean ± S.D of 3 individual tumors (n=3), with each dot representing a biological replicate. Statistical significance was determined by Unpaired student t-tests (*p<0.05, **p<0.005). All images were taken at 20X magnification. Scale bar = 50μm.

(D) ***SA fibroblast-derived matrices contain lower levels of FN and decreased FN expression is associated with higher levels of Smad7.*** WT and SA primary fibroblast-derived matrices were evaluated for their expression of FN and Smad7 by IF. Representative IF images are shown here. Fluorescence intensity of FN staining is presented as the mean ± S.D. of 6 independent experiments with each dot representing a biological replicate. Statistical significance was determined by Unpaired t tests (**p<0.005, n=6). The percentage of SMAD7-positive nuclei is presented as the mean ± S.D. of 3 independent experiments with each dot representing a biological replicate. Statistical significance was determined by Unpaired t-test (*p<0.05; n=3). All images were taken at 20X magnification. Scale bar = 50μm.

(E) ***IFN1 induces Smad7 expression in WT fibroblasts.*** NIH3T3 cells were serum-starved (0.1% BSA-DMEM) overnight, then pre-treated with 2000U/mL IFNβ for 2 hours and stimulated with 2.5 ng/ml TGFβ1 for an additional 4 hours. Cells were treated with PBS as a control. Whole cell lysates evaluated for expression of SMAD7 by Western blot analysis. GAPDH was used as a loading control. The numbers below each protein band indicates the integrated density of that band, with PBS-treated control set to 1. A representative blot is shown here (n=3).

(F) ***Knockdown of Smad7 rescues the ability of SA fibroblasts to generate FN-expressing matrix.*** Matrices generated by SA lung fibroblasts infected with lentiviruses carrying either empty vector (CTRL) or shRNA against SMAD7 (shSMAD7) were evaluated for the expression of FN or Smad7 by IF. Fluorescence intensity of FN staining is shown as the mean ± S.D. of 3 independent experiments (n=3) with each dot representing a biological replicate. The percentage of SMAD7-positive nuclei is presented as the mean ± S.D. of 3 independent experiments (n=3) with each dot representing a biological replicate. Statistical significance was determined by Unpaired t-test (*p<0.05). All images were taken at 20X magnification. Scale bar = 50μm.

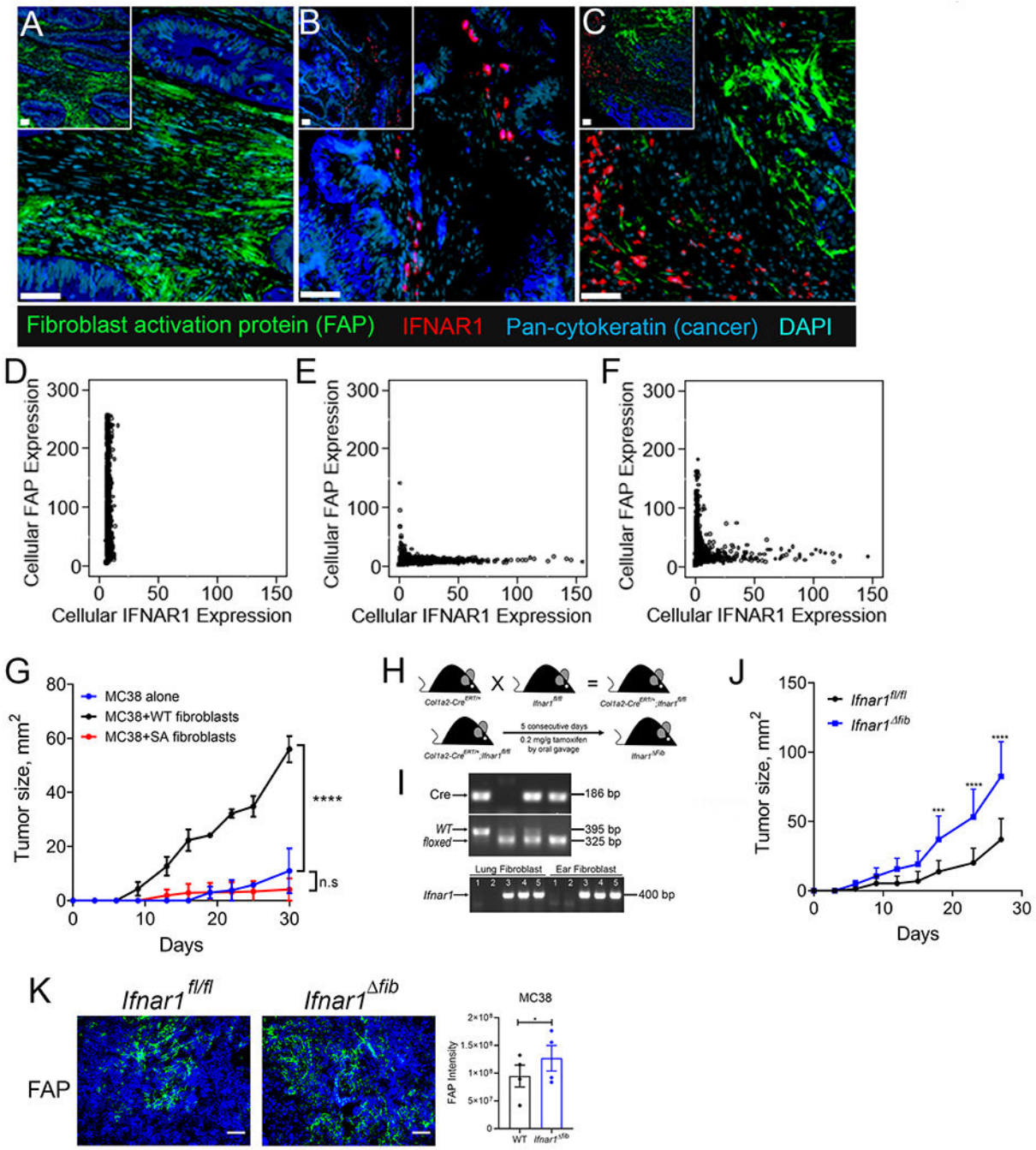

Figure 3. Inactivation of type I IFN signaling in CAFs promotes tumor growth.

(A-F) Intratumoral FAP expression is limited to regions largely absent of IFNAR1 in human CRC tumor tissues. Human CRC tumors (total of n=150) were evaluated for expression of IFNAR1 (red) and FAP (green) by IF. Malignant cells were stained with pan-cytokeratin (blue) and cell nuclei were stained with DAPI (teal). Scale bar=50μm; the inserts show lower magnification with larger tumor context. Quantification of FAP and IFNAR1 levels was completed using Tissue Studio image analysis software. User-guided machine learning was used for cell segmentation and identification of epithelial or stromal

compartments of each tissue facilitated by DAPI-stained cell nuclei and pan-cytokeratin-stained cancer cells. Mean cell signal intensity of FAP and IFNAR1 was computed for epithelial and stromal regions. Scatterplots of single cell IFNAR1 and FAP signal intensities within the stromal compartment were generated per patient tumor core. Representative cases are shown that illustrate the generally mutual exclusivity of cellular FAP and IFNAR1 by predominantly FAP+/IFNAR1− tumors (Panels **A** and **D**), predominantly FAP−/IFNAR1+ (Panels **B** and **E**), or mixed FAP+/IFNAR1+ tumors (Panels **C** and **E**).

(G) Growth of MC38 tumors is enhanced when cancer cells are co-injected with WT, but not SA fibroblasts. Mice were inoculated with 10^5 MC38 cells alone (n=7), or with mixtures of 10^5 MC38 cells and 10^4 WT (n=9) or SA (n=5) fibroblasts. Each point in the line graphs represents the mean ± S.D tumor area (mm^2). Statistical significance was determined by Two-way ANOVA and Sidak's post-hoc test (****p<0.0001, n.s=not significant).

(H) A schematic outlining the generation Ifnar1$^{\Delta fib}$ mice. *Col1a2-Cre*$^{ERT2/+}$ mice were crossed with *Ifnar1*$^{fl/fl}$ mice to generate *Col1a2-Cre*$^{ERT2/+}$; *Ifnar1*$^{fl/fl}$ mice. *Col1aI2-Cre*$^{ERT2/+}$; *Ifnar1*$^{fl/fl}$ mice were administered with tamoxifen (0.2 mg/g by oral gavage for 5 consecutive days). The resultant mice were called *Ifnar1*$^{\Delta fib}$ mice.

(I) Genotyping of Col1a2-Cre$^{ERT2/+}$; Ifnar1$^{fl/fl}$ mice (left) and validation of IFNAR1 ablation (right). Genomic DNA from 4 mice were evaluated for expression of *Col1a2-Cre*$^{ERT2/+}$ (top gel) and *Ifnar1*$^{fl/fl}$ (middle gel). A single band at 186bp indicated the presence of *Col1a2-Cre*$^{ERT2/+}$. The floxed allele of *Ifnar1* is represented by a band at 325, and the WT allele is represented by a band at 395bp. The presence of double bands at 325bp and 395 bp is indicative of a heterozygote. After tamoxifen treatment, mice were euthanized, and lung and ear fibroblasts were evaluated for *Ifnar1* deletion by PCR (bottom gel). The absence of a band at 400bp indicates that *Ifnar1* has been deleted. Thus, mice 1 and 2 are *Ifnar1*$^{\Delta fib}$, while mice 3-5 are *Ifnar1*$^{fl/fl}$.

(J) Conditional inactivation of IFNAR1 in fibroblast enhances tumor growth. Mice were inoculated with 10^5 MC38 cells. Each point in the line graphs represents the mean ± S.D tumor area (mm^2) of 5 mice (n=5 for *Ifnar1*$^{\Delta fib}$ and *Ifnar1*$^{fl/fl}$). Statistical significance was determined by Two-way ANOVA and Sidak's post-hoc test (***p<0.005; ****p<0.0005).

(K) Tumors from experiment described in panel J were allowed to reached equal maximal size (~200 mm^2) and then were harvested and analyzed for FAP expression. The expression levels of FAP and SMAD7 in *Ifnar1*$^{\Delta fib}$ and *Ifnar1*$^{fl/fl}$ tumors were evaluated by IF. Fluorescence intensity is presented as mean ± S.D of 4 individual tumors (n=4), with each dot representing a biological replicate. Statistical significance was determined by Paired ratio t-tests (*p<0.05). All images were taken at 20X magnification. Scale bar = 50μm.